Supporting Information

A Robust Sulfonate-Based Metal-Organic Framework with Permanent Porosity for Efficient CO_2 Capture and Conversion

Guiyang Zhang,[†] Guangfeng Wei,[†] Zhipan Liu,[⊥] Scott R. J. Oliver,[‡,*] and Honghan Fei[†,*]

[†]Department of Chemistry, Shanghai Key Laboratory of Chemical Assessment and Sustainability, Tongji University, Shanghai 200092, P. R. China

[‡]Department of Chemistry and Biochemistry, University of California, Santa Cruz, 1156 High Street, Santa Cruz, California 95064, United States

[⊥]Collaborative Innovation Center of Chemistry for Energy Material, Shanghai Key Laboratory of Molecular Catalysis and Innovative Materials, Key Laboratory of Computational Physical Science (Ministry of Education), Department of Chemistry, Fudan University, Shanghai 200433, China

*To whom correspondence should be addressed.

[†]E-mail: fei@tongji.edu.cn

[‡]E-mail: soliver@ucsc.edu

General Methods

Starting materials and solvents were purchased and used without further purification from commercial suppliers (Sigma-Aldrich, Alfa Aesar, TCI, and others). Proton nuclear magnetic resonance spectra (^{1}H NMR) were recorded on a Varian FT-NMR spectrometer (400 MHz). Chemical shifts were quoted in parts per million (ppm) referenced to the appropriate solvent peak or 0 ppm for TMS. Elemental analysis (EA) for C, H, and N were operated on a FLASH EA 1112 element analyzer. Thermogravimetric analysis (TGA) were carried out in N_2 stream (60 mL/min) on a NETZSCH STA 409 PC/PG differential thermal analyzer running from room temperature to 800 °C with a heating rate of 10 °C/min. Fourier-transform infrared (FT-IR) spectra were recorded using a Nicolet iS10 spectrophotometer with KBr pellets in 4000~400 cm^{-1} region. $[Cu_2(bpy)(bdc)_2]_n$ was prepared according to the procedure in the literature[s1] and the phase purity was confirmed by powder X-ray diffraction and gas adsorption (Figure S4 and S13).

Experimental Section

Hydrothermal Synthesis of TMOF-1. A mixture of 0.34 g $Cu(NO_3)_2 \cdot 3H_2O$ (1.4 mmol), 0.22 g 4,4'-bipyridine (bpy 1.4 mmol), 0.33 g disodium 1,2-ethanedisulfonate ($EDSNa_2$, 1.4 mmol), and 10 mL deionized water were added into a 15 mL Teflon-lined autoclave reactor followed by 30 min sonication for sufficient dispersion. The autoclave was then sealed into a stainless steel vessel and heated at 175 °C for 72 h, which was then cooled down to room temperature at a rate of 6 °C/h. Dark blue cubic crystals (Figure S14) of TMOF-1 suitable for single-crystal X-ray diffraction were collected by filtration. The crystals were rinsed with distilled water (2×20 mL), acetone (2×20 mL) and dried in air, giving a yield of 75% (0.29 g) based on bpy. Elemental analysis calculated for $CuC_{22}H_{20}N_4O_6S_2$: C, 46.84; H, 3.57; N, 9.93, found: C, 46.17; H, 3.85; N, 9.90 (%, after activation).

Bulk Synthesis of TMOF-1. A mixture of 1.55 g $Cu(NO_3)_2 \cdot 3H_2O$ (6.40 mmol), 1.00 g bpy (6.4 mmol), and 1.50 g $EDSNa_2$ (6.4 mmol) were added into 100 mL deionized water, and the mixture was refluxed for 48 hours. After completion of the reaction, the mixture was filtered and the residue was collected, rinsed with distilled water (2×20 mL), acetone (2×20 mL), and dried in air to give uniform blue powders of TMOF-1 with a yield of 62 % (1.11 g) based on bpy.

Powder X-ray Diffraction. ~20 mg TMOF-1 sample was dried under vacuum prior to PXRD analysis. PXRD data was collected at ambient temperature on a Bruker D8 Advance diffractometer at 40 kV, 40 mA for Cu Kα (λ = 1.5418 Å), with a scan speed of 1 sec/step, a step size of 0.02° in 2θ, and a 2θ range of 5~40°. The experimental backgrounds were corrected using JADE 5.0 software package.

Single Crystal X-ray Diffraction. A single crystal of TMOF-1 suitable for X-ray analysis was chosen under an optical microscope, and mounted onto a glass fiber. The diffraction data were collected at 150(2) K using graphite-monochromated Mo-Kα radiation (λ = 0.71073 Å) from a fine-focus sealed tube operated at 50 kV and 30 mA on a Bruker SMART APEX II CCD area detector X-ray diffractometer. The structure was solved by direct methods and expanded routinely. The model was refined by full-matrix least-squares analysis of F^2 against all reflections. All non-hydrogen atoms were refined with anisotropic thermal displacement parameters. Thermal parameters for hydrogen atoms were tied to the isotropic thermal parameter of the atom to which they are bonded. Programs used were APEX-II v2.1.4,[s2] SHELXTL v6.14,[s3] and Diamond v3.1e.[s4] Further details of crystallographic data and structural refinement are summarized in Table S1. CCDC 1479446 contains the supplementary crystallographic data for TMOF-1. These data can be obtained freely from the Cambridge Crystallographic Data Centre *via* www.ccdc.cam.ac.uk/data_request/cif.

Activation of TMOF-1. Freshly prepared crystals were soaked in 20 mL methanol

(MeOH) for 3 days over which the solvent was exchanged with fresh MeOH (20 mL) every 12 h. Then, the crystals were filtrated, and dried overnight under vacuum at 105 °C.

Gas Sorption. ~150 mg of activated TMOF-1 was transferred to a pre-weighed sample tube and degassed at 105 °C on a Micromeritics ASAP 2020 adsorption analyzer for a minimum of 12 h or until the outgas rate was less than 5 mm Hg. The sample tube was re-weighed to obtain a consistent mass for the degassed sample. Brunauer-Emmett-Teller (BET) surface area data were collected volumetrically at 87 K by Ar and 77K by N_2. The exact surface area was averaged by the analyses of three independent samples. H_2 sorption experiments were performed at 77K and 87K by liquid N_2 bath and liquid Ar bath, respectively. CO_2 sorption experiments were performed at 200K, 273K, 298K, and 308K by dry ice-ethanol bath, ice-water bath and heating jacket, respectively. Isosteric heat of adsorption (Q_{st}) for H_2 or CO_2 were calculated by applying the Clausius-Clapeyron equation to two sets of adsorption data collected at two variable temperatures.

TMOF-1 Thermal and Chemical Stability Studies. ~100 mg of as-synthesized TMOF-1 were fully activated at 110 °C under vacuum, followed by incubation under the specified condition (*e.g.* boiling organic solvents, boiling water, acid/base condition or heating in air) for 24 hours. Then, the TMOF-1 were isolated by filtration, air-dried, and re-activated at 110 °C under vacuum before performing PXRD and mass balance measurements.

Catalysis for CO_2 Conversion. In each individual reaction, 20 mmol epoxide substrate along with 0.11 g TMOF-1 catalyst (1 mol% based on Cu(II)) and 0.65 g tetra-*n*-*tert*-butylammonium bromide co-catalyst (TBAB, 10 mol%) were added into a Schlenk tube. The tube was purged with CO_2 at 1 atm under solvent free environment at room temperature and fixed onto a mechanical shaker with a constant shaking rate of 200 c.p.m. for 48 h to complete the catalytic reaction. The mixture

was then filtrated, and the filtrate was characterized by ^{1}H-NMR spectra to quantitatively verify the product (Figure S15). Chemical shifts were quoted in parts per million (ppm) referenced to the appropriate solvent peak or 0 ppm for tetramethylsilane (TMS).

Calculation Details

All DFT calculations were performed using VASP package[s5] with projected augmented wave (PAW) pseudo-potentials[s6, s7]. The exchange–correlation energy was treated based on the generalized gradient approximation (GGA) by using Perdew–Burke–Ernzerhof (PBE) functional[s8]. The plane-wave cutoff energy was set to 400 eV, and the Monkhorst-Pack k-point mesh was utilized for first Brillouin zone integrations. In this work, a (2×2×2) k-point were applied for the CO_2 adsorption calculations in TMOF-1 (the unit cell size: 15.8Å×15.8Å×11.3Å). The DFT-D3(BJ) method of Grimme[s9, s10] were employed to describe long-range vdW interactions between CO_2 and the TMOF-1 skeleton. All atoms were fully relaxed until the total energy difference between two ionic steps is less than 10^{-3} eV.

We are able to obtain the adsorption free energy of CO_2 (ΔG_{ad}) through the following equations (Eq. S1-3).

$$\mathbf{G_{ad} = E_{ad} - T \cdot S + ZPE} \quad \text{(S1)}$$

$$\mathbf{G_{CO2} = E_{CO2} - T \cdot S^0_{CO2} + \Delta H_{(0\sim298K)}} \quad \text{(S2)}$$

$$\mathbf{\Delta G_{ad} = G_{ad} - G_{CO2} - E_{TMOF\text{-}1}} \quad \text{(S3)}$$

By adding CO_2 to various places inside the TMOF-1 skeleton, the energy of the adsorption states (E_{ad}) are directly available from DFT calculations. The Eq. S1 shows that the free energy of the adsorption states (G_{ad}) can be obtained after the correction of vibrational entropy (S) and the zero-point energy (ZPE). The free energy of gaseous CO_2 (G_{CO2}) is -0.56 eV refer to the free energy of CO_2(E, 0 K)[s11], which

can be found in the standard thermodynamic data[s12] (Eq. S2). ΔG_{ad} can then be calculated by using Eq. S3.

For the first principle molecular dynamics simulation, the Nosé algorithm was used with a timestep of 1 fs within the canonical ensemble. A 15 ps NVT simulation is reported which was first equilibrated for 3 ps with a Nosé-Hoover thermostat at 300 K. A single unit cell of TMOF-1 was used for all DFT calculations with Γ-point sampling of the Brillouin zone.

Supporting Figures and Tables

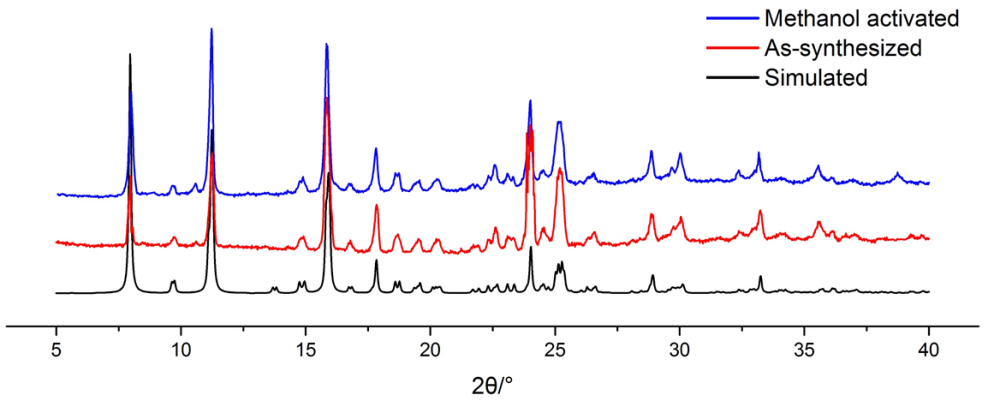

Figure S1. PXRD patterns of TMOF-1: simulated, as-synthesized, and methanol activated.

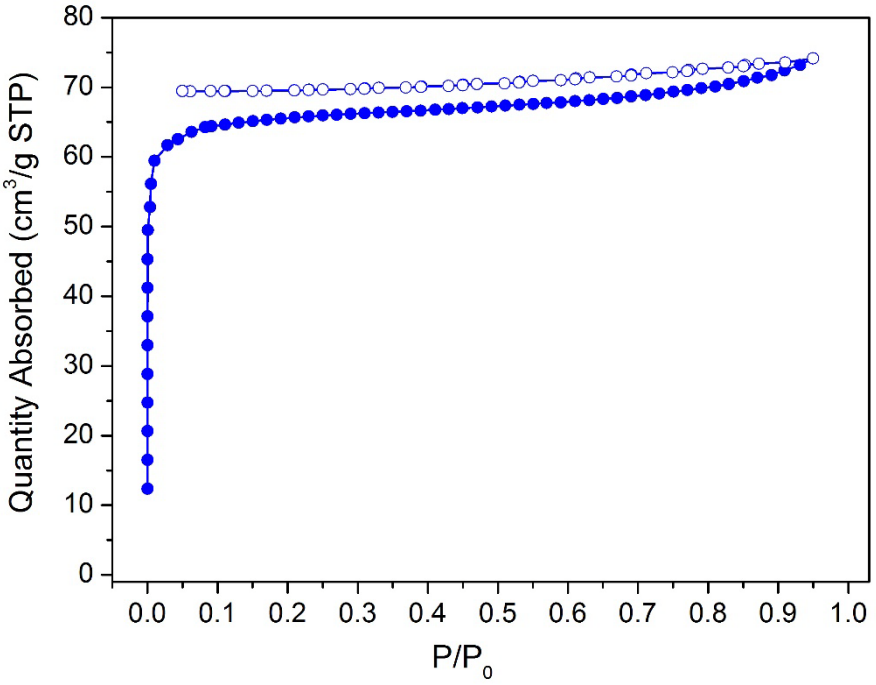

Figure S2. N_2 sorption isotherm of TMOF-1 at 77K.

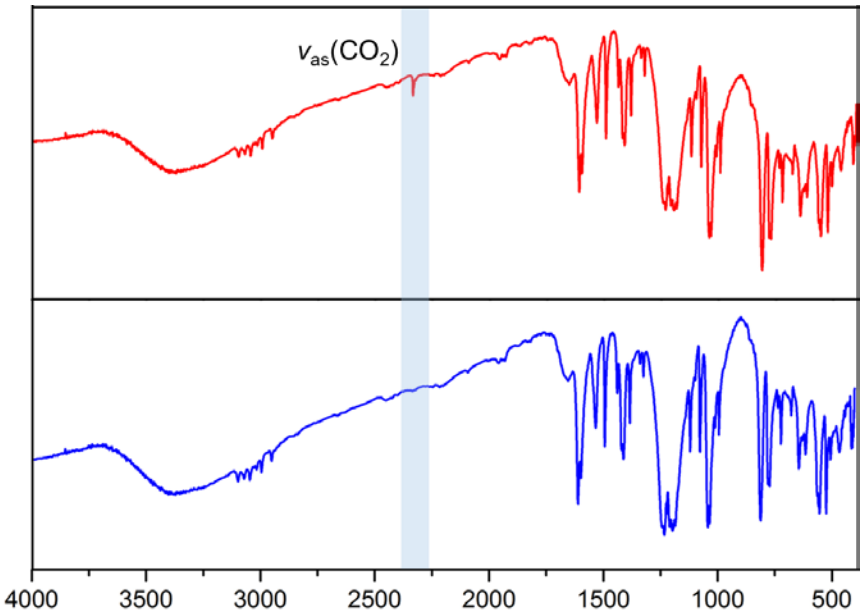

Figure S3. FT-IR spectra of TMOF-1: before (blue) and after (red) CO_2 adsorption at room temperature.

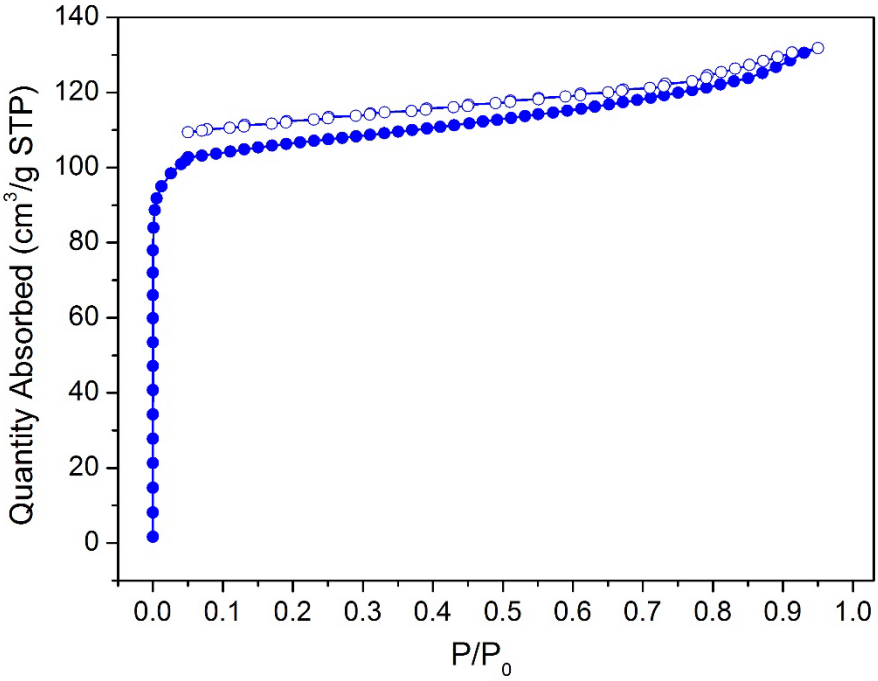

Figure S4. Ar sorption isotherm of $[Cu_2(bpy)(bdc)_2]_n$ at 87K.

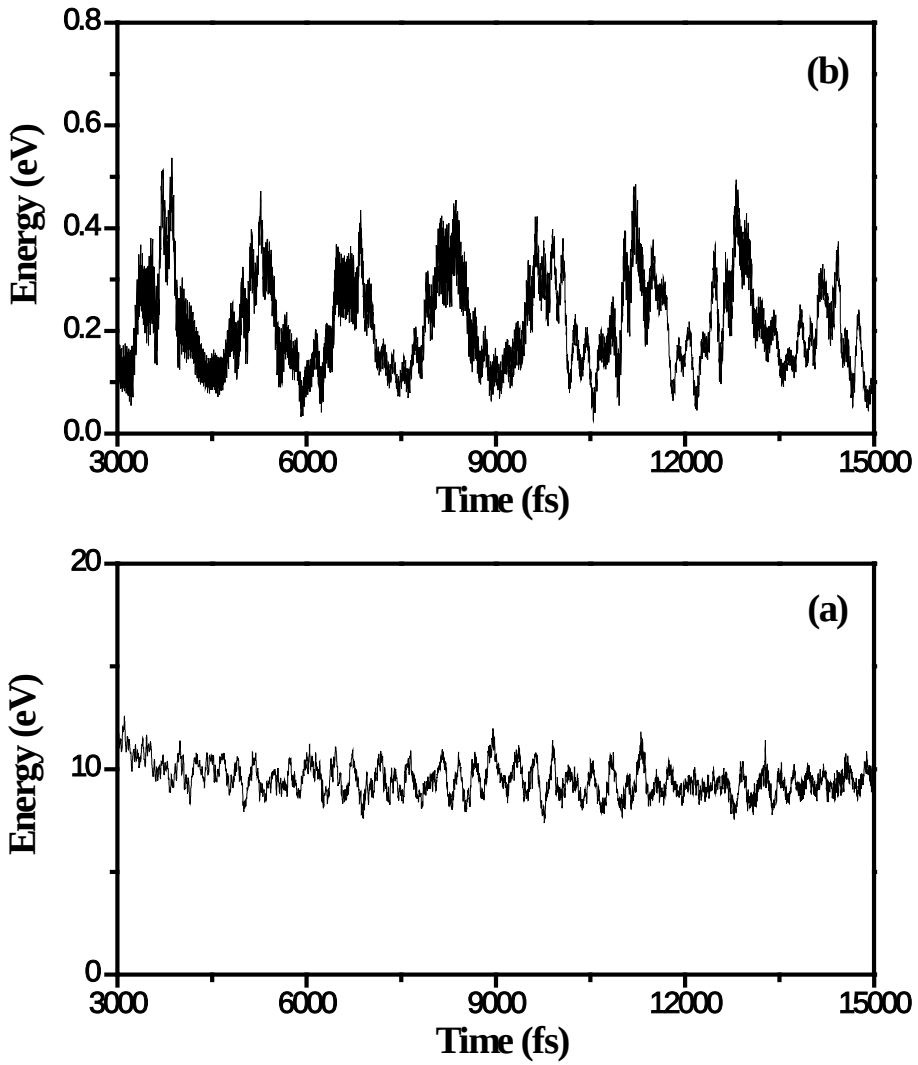

Figure S5. The molecular dynamics (MD) simulation of CO_2 adsorbed TMOF-1 (two CO_2 adsorbed per unit cell) at 300K. In the 15 ps, the CO_2 and the TMOF-1 skeleton always stay around the most stable adsorption sites (see Figure 5). (a) The MD simulation with the TMOF-1 skeleton being fixed; (b) the MD simulation with all atoms being fully relaxed.

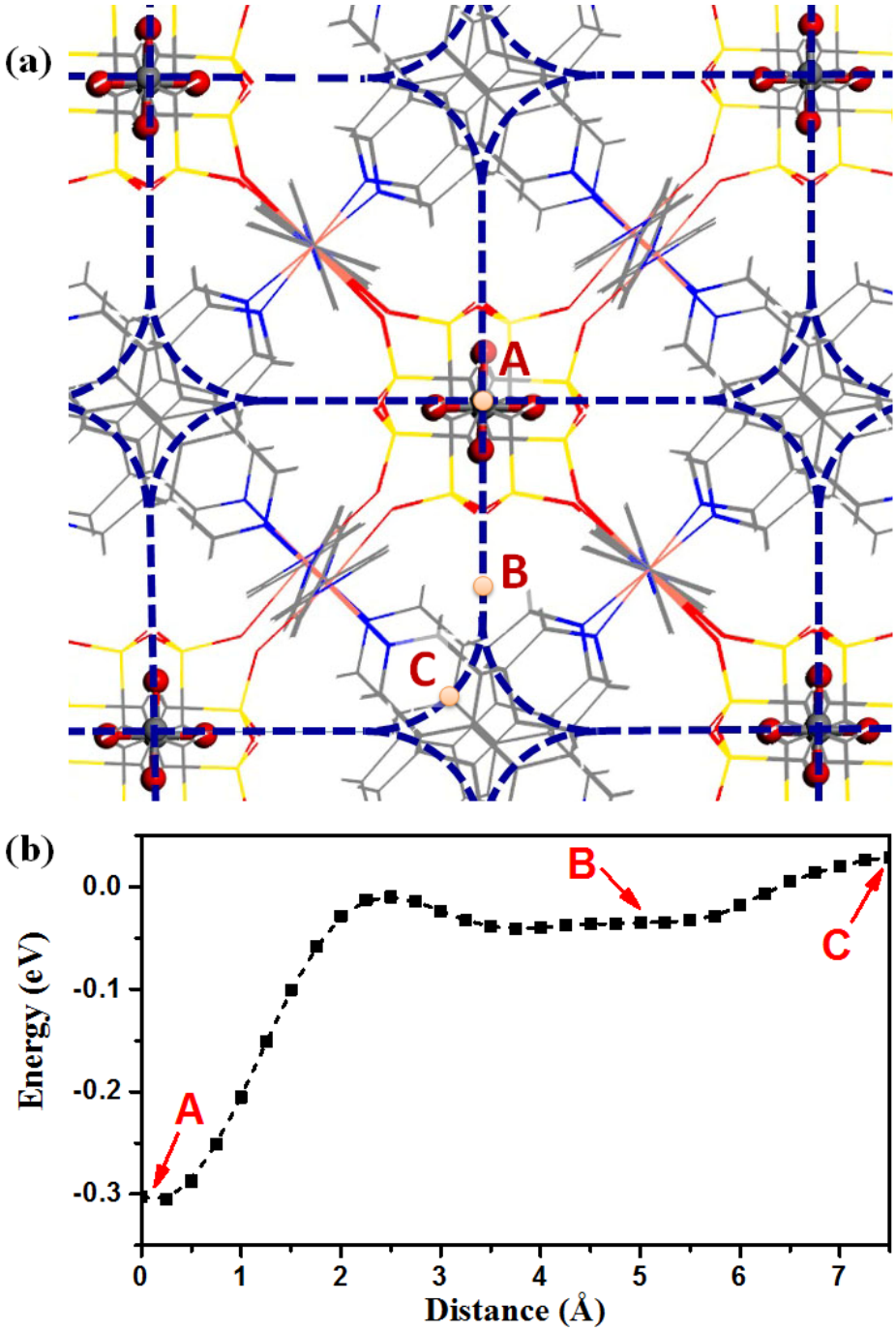

Figure S6. (a) The proposed CO_2 diffusion channels (blue dashed lines) along the 3D interconnected porosity of TMOF-1. We highlighted three different positions on the CO_2 diffusion channel. Position A is the most stable CO_2 adsorption site, position B is the second stable CO_2 adsorption site and position C is the middle place of the diffusion channel. (b) The energy difference (ΔE, refer to the energy of gas phase CO_2 and activated TMOF-1) of the system during a CO_2 molecule moving from position A to positon C. The barrier for CO_2 diffusion within TMOF-1 is ~0.33 eV.

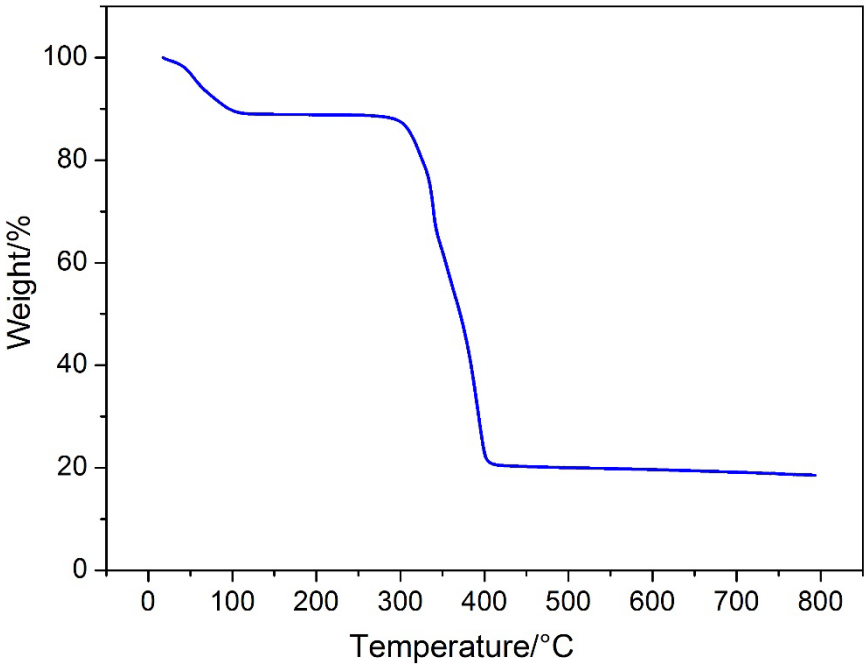

Figure S7. Thermogravimetric analysis curve of TMOF-1 in N_2 flow.

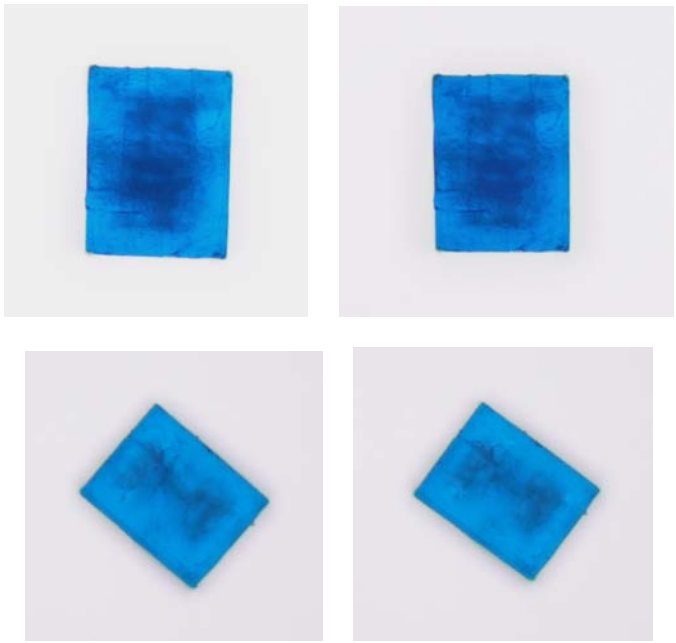

Figure S8. Top: *In-situ* optical microscope image of TMOF-1 (~100 × 80 × 80 μm size crystal) before (left) and after (right) incubation in pH=3 solution (HCl/H_2O) for 24 h. Bottom: *In-situ* optical microscope image of TMOF-1 (~100 × 80 × 80 μm size crystal) before (left) and after (right) incubation in pH=10 solution ($NaOH/H_2O$) for 24 h.

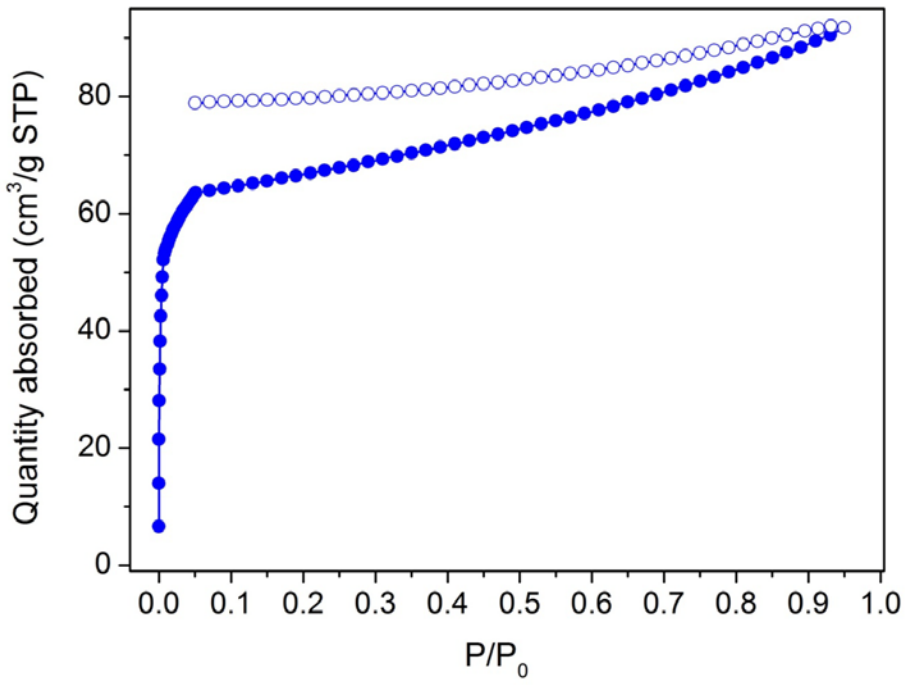

Figure S9. Ar sorption isotherm (at 87K) of TMOF-1 after refluxing in water for 24 h.

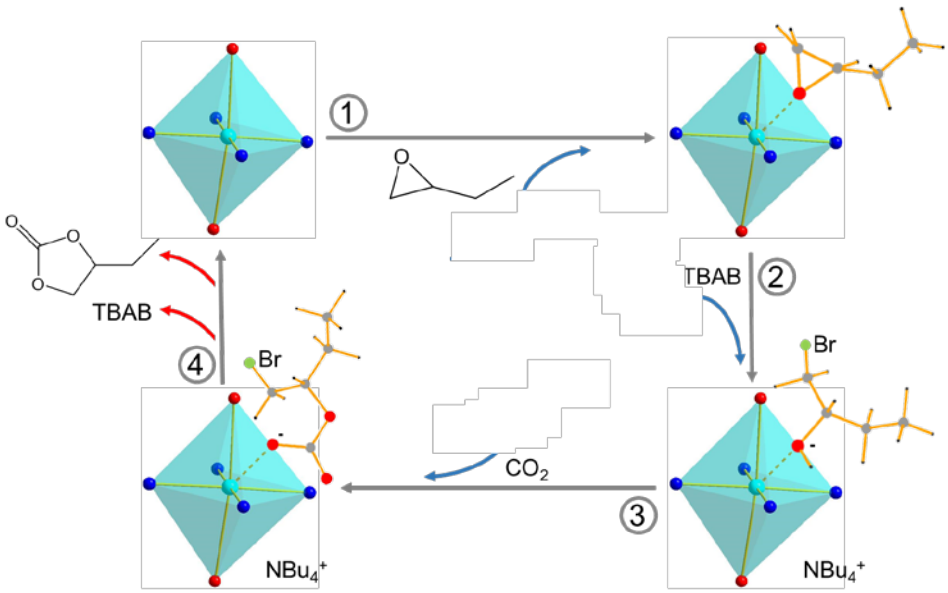

Figure S10. Presumable mechanism of the CO_2 cycloaddition reaction catalyzed by TMOF-1 along with TBAB.

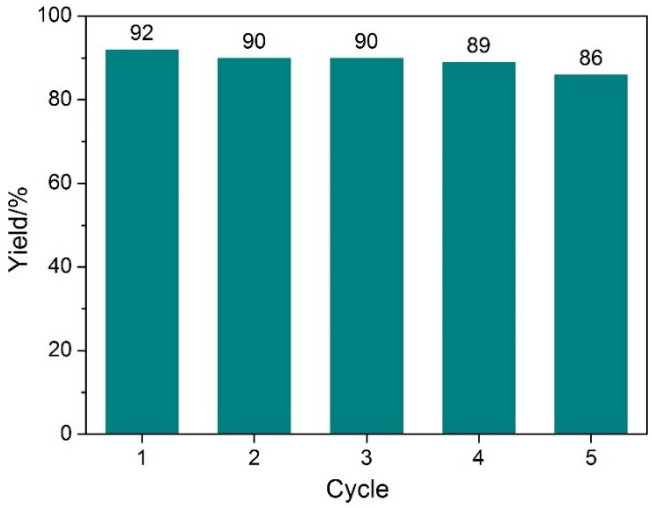

Figure S11. Recyclability of TMOF-1 in five successive runs of the catalytic reaction using 2-(chloromethyl)oxirane as substrate.

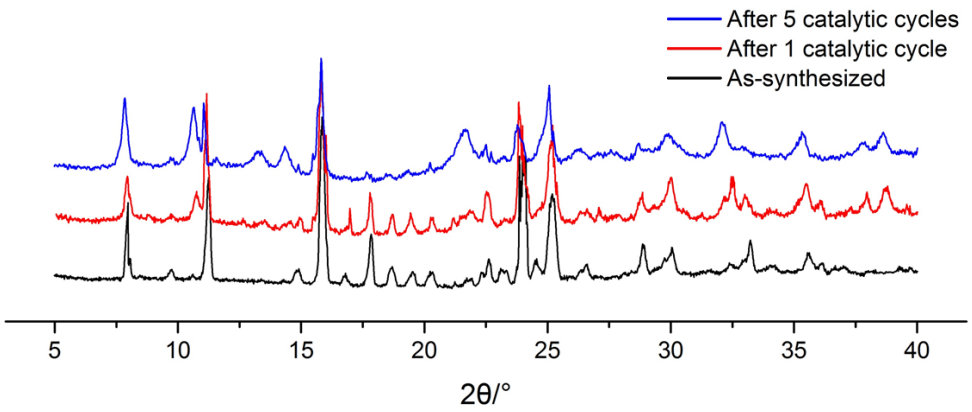

Figure S12. PXRD patterns of TMOF-1: as-synthesized, after 1 catalytic cycle, and after 5 catalytic cycles.

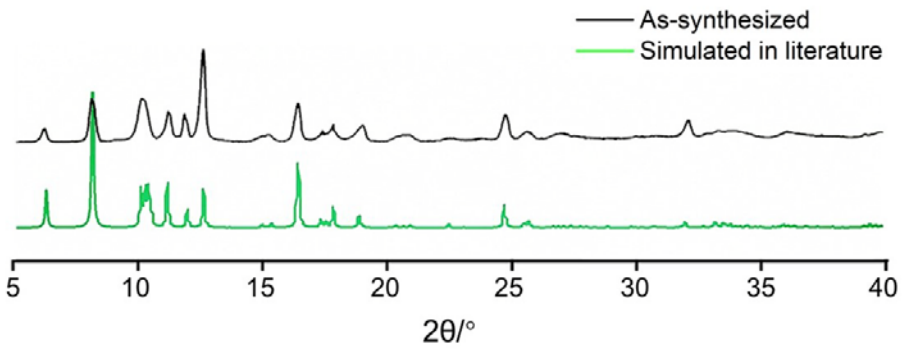

Figure S13. PXRD patterns of $[Cu_2(bpy)(bdc)_2]_n$: as-synthesized and simulated in the literature.

Figure S14. Optical microscope image of a TMOF-1 single crystal.

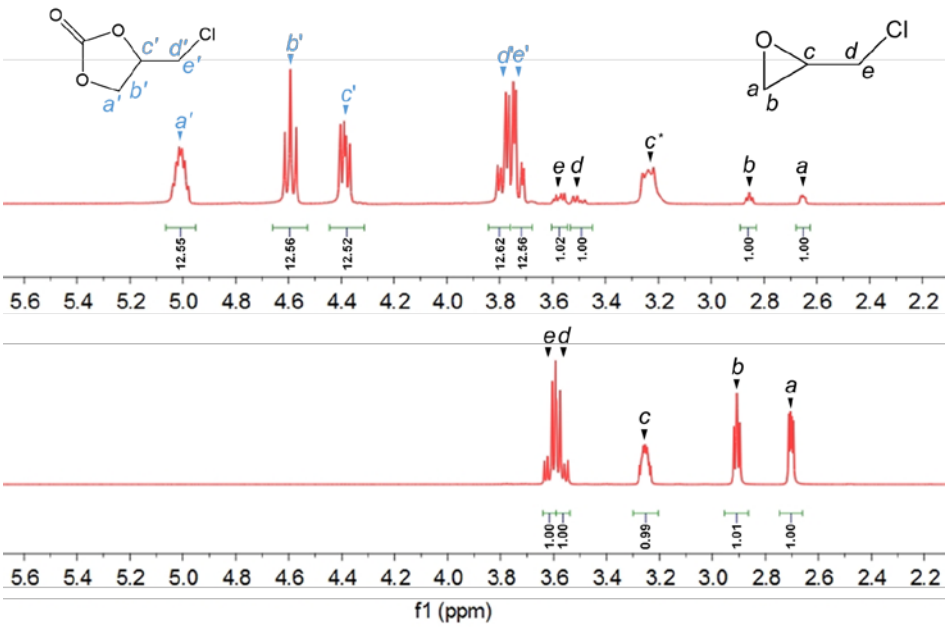

Figure S15. ^{1}H-NMR spectra of an epoxide substrate before (down) and after (up) a 48-hour CO_2 cycloaddition reaction; c^*: partly overlapped with a peak of TBAB.

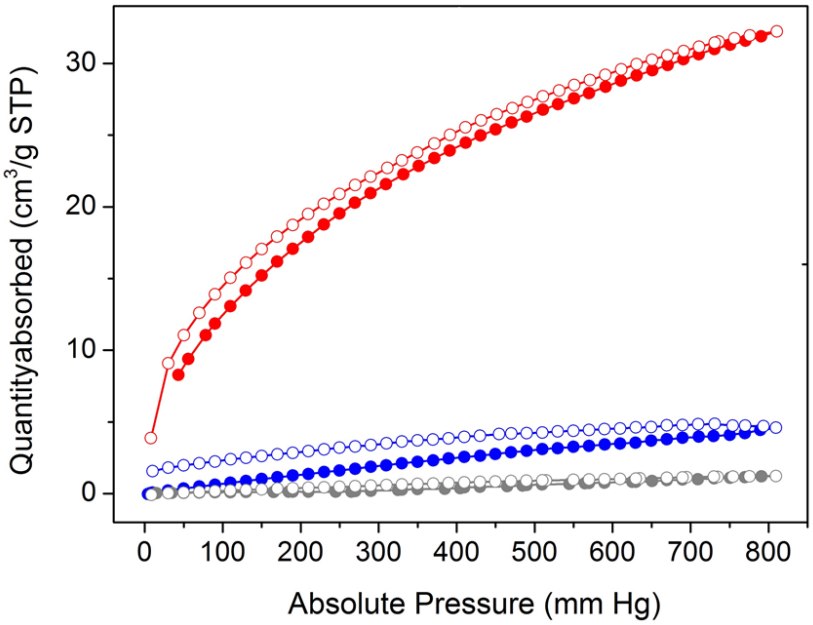

Figure S16. CO_2 (red), N_2 (grey), and O_2 (red) sorption isotherm of TMOF-1 at 298K. Overall, CO_2 is the most strongly adsorbed molecule due to its large quadrupolar moment. Importantly, a relatively steep increase was observed at low pressure (e.g. 13 cm^3/g at 100 mmHg), indicating its strong interaction with sulfonate functional groups. However, no apparent adsorption (< 5 cm^3/g at 1 bar) of N_2 or O_2 was observed under the same condition. Based on these results, we conclude that the material can selectively absorb CO_2 in presence of N_2 and O_2 at room temperature.

Table S1. Mass balance of TMOF-1 before and after thermal and chemical treatment.

Condition	Initial mass (mg)	Final mass (mg)	Wt. Loss (%)
Boiling water	101.2	92.6	8.5
Boiling methanol	100.5	96.9	3.6
Boiling hexane	102.2	97.5	4.5
pH=10 ($NaOH/H_2O$)	102.1	97.1	4.9
pH=3 (HCl/H_2O)	100.9	96.3	4.6
In air at 260 °C	101.1	95.1	5.9

Table S1. Crystal data and structure refinement for TMOF-1.

Identification code	TMOF-1	
Empirical formula	$C_{22}H_{20}CuN_4O_6S_2$	
Formula weight	564.09	
Temperature	150(2) K	
Wavelength	0.71073 Å	
Crystal system	Monoclinic	
Space group	C2	
Unit cell dimensions	a = 22.28(2) Å	α = 90°
	b = 22.20(2) Å	β = 90.931(8)°
	c = 11.198(10) Å	γ = 90°
Volume	5539(9) $Å^3$	
Z	6	
Density (calculated)	1.353 g/cm^3	
F(000)	2312	
Crystal size	0.08 × 0.07 × 0.05 mm^3	
θ range for data collection	2.22 ~ 27.48°	
Limiting indices	$-28 \le h \le 28$, $0 \le k \le 28$, $0 \le l \le 14$	
Reflections collected	6496	
Independent reflections	5653	
Completeness to θ = 27.48°	99.5 %	
Absorption correction	Empirical	
Max. and min. transmissions	0.7456 and 0.6761	
Data / restraints / parameters	6496 / 1 / 636	
Goodness-of-fit on F^2	1.052	
Final R indices [I > 2σ (I)]	R_1 = 0.0371, wR_2 = 0.0916	
R indices (all data)	R_1 = 0.0444, wR_2 = 0.0951	
Largest diff. peak and hole	0.546 and -0.374e.$Å^{-3}$	

References

S1. Sumida, K.; Moitra, N.; Reboul, J.; Fukumoto, S.; Nakanishi, K.; Kanamori, K.; Furukawa, S.; Kitagawa, S., *Chem. Sci*. **2015,** 6, 5938-5946.

S2. *APEX-II*, *2.1.4*, Bruker-AXS: Madison, WI, 2007.

S3. *SHELXTL*, *Crystal Structure Determination Package*, Bruker Analytical X-ray Systems Inc.: Madison, WI, 1995~99.

S4. Brandenburg, K.; Putz, H., Diamond, *Crystal Impact*, Bonn, Germany, 2007.

S5. Kresse, G.; Furthmuller, J., *Comput. Mater. Sci.* 1996, 6, 15-50.

S6. Blochl, P. E., *Phys. Rev. B* 1994, 50, 17953-17979.

S7. Kresse, G.; Joubert, D., *Phys. Rev. B* 1999, 59, 1758-1775.

S8. Perdew, J. P.; Burke, K.; Ernzerhof, M., *Phys. Rev. Lett.* 1996, 77, 3865-3868.

S9. Grimme, S.; Antony, J.; Ehrlich, S.; Krieg, H., *J. Chem. Phys.* 2010, 132, 154104.

S10. Grimme, S.; Ehrlich, S.; Goerigk, L., *J. Comput. Chem.* 2011, 32, 1456-1465.

S11. Liu, Z. P.; Jenkins, S. J.; King, D. A., *J. Am. Chem. Soc.* 2004, 126, 10746-10756.

S12. *CRC Handbook of Chemistry and Physics*; 84 ed.; R.LIDE, D., Ed.; CRC press, 2003-2004.